

Photophysical comparison of liquid and mechanically exfoliated WS₂ monolayers

Zhaojun Li^{1,2}, Farnia Rashvand³, Hope Bretscher¹, Beata M. Szydłowska³, James Xiao¹, Claudia Backes^{3,4}, Akshay Rao^{1*}

¹Cavendish Laboratory, University of Cambridge, JJ Thomson Avenue, CB3 0HE, Cambridge, United Kingdom

²Molecular and Condensed Matter Physics, Department of Physics and Astronomy, Uppsala University, 75120 Uppsala, Sweden

³Institute for Physical Chemistry, Ruprecht-Karls-Universität Heidelberg, Im Neuenheimer Feld 253, 69120 Heidelberg, Germany

⁴Current address: Physical Chemistry of Nanomaterials, University of Kassel, Heinrich-Plett-Str.40, D-34132 Kassel, Germany

*Corresponding author

Contact e-mail: ar525@cam.ac.uk

Keywords: Tungsten disulphide, liquid phase exfoliation, energy transfer, exciton dynamics

Abstract

Semiconducting transition metal dichalcogenides (TMDs) are desired as active materials in optoelectronic devices due to their strong excitonic effects. They can be exfoliated from their parent layered materials with low-cost and for mass production *via* a liquid exfoliation method. However, the device application of TMDs prepared by liquid phase exfoliation is limited by their poor photoluminescence quantum efficiencies (PLQE). It is crucial to understand the reason to low PLQE for their practical device development. Here we evaluate the quality of monolayer-enriched liquid phase exfoliated (LPE) WS₂ dispersions by systematically investigating their optical and photophysical properties and contrasting with mechanically exfoliated (ME) WS₂ monolayers. An in-depth understanding of the exciton dynamics is gained with ultrafast pump-probe measurements. We reveal that the energy transfer between monolayer and few-layers in LPE WS₂ dispersions is a

substantial reason for their quenched PL. In addition, we show that LPE WS₂ is promising to build high performance optoelectronic devices with excellent optical quality.

Introduction

The study of transition metal dichalcogenides (TMDs) has become a vibrant area in nanomaterial science.^{1,2} Exfoliated TMDs have been widely used in the field of optoelectronics due to their excellent light absorptivity and semiconducting performance.³⁻⁶ To utilize TMD materials, achieving more scalable techniques is critically important, and considerable effort has been devoted to the development of cost-effective mass production methods.^{7,8} Although mechanical exfoliation produces the highest quality materials, its application is limited by extremely low and uncontrollable yield.^{9,10} In contrast, liquid exfoliation yields atomically thin TMD flakes in a liquid medium in large quantities at moderate cost.^{11,12} The simplest way to produce nanosheets suspended in liquid is termed liquid phase exfoliation (LPE) which relies on immersing the bulk materials into suitable solvents or aqueous surfactant solution and apply high energy, *e.g.* sonication, to achieve exfoliation accompanied with tearing.^{13,14} When appropriately chosen, the solvent or surfactant suppresses reaggregation in the liquid.¹⁵ This approach is widely applicable to a range of materials and takes advantage of well-established print production processes for new generation of device fabrication.^{16,17} Nevertheless, liquid-exfoliated (LE) TMD nanosheets have been rarely used in optoelectronics, which is often attributed to their poor quality, such as defects, impurities, nonuniformity and small size, resulting in low photoluminescence quantum efficiencies (PLQE).¹⁸ Hence the development of high PLQE LE TMD monolayers is of fundamental importance toward the practical implementation of optoelectronic devices with TMDs. Nowadays, the quality of the LPE TMDs is improving with the continual development of the liquid phase exfoliation methodology and subsequent size selection.¹⁹ Largely defect-free monolayer enriched TMD dispersions with narrow line width photoluminescence (PL), which are similar to that of mechanically-exfoliated (ME) TMDs, were demonstrated.^{20,21} However, the PLQE of LPE TMD dispersions remains low and exciton dynamics of TMD dispersions is only little explored.²² In particular, most reports focus on ensembles with low monolayer content produced either from LPE or colloidal synthesis.²³⁻²⁶ Recently, we achieved high quality WS₂ samples by mechanical exfoliation with bis(trifluoromethane)sulfonimide lithium salt (Li-TFSI) surface treatment, showing superior PL. In this work, we evaluate the quality of monolayer enriched WS₂ dispersion produced from liquid phase exfoliation by conducting a systematic study on the optical and photophysical properties of different LPE WS₂ dispersions and ME WS₂ monolayer samples. The LPE WS₂ dispersions can achieve PL with narrow linewidth and almost no Stoke shift compared to their absorption spectra. In addition, we use ultrafast pump-probe spectroscopy to study

the exciton dynamics following photoexcitation in these WS₂ samples. We reveal that the energy transfer between monolayers and few-layers in LPE WS₂ dispersion samples can be a major factor for their quenched PL.

Results and Discussion

The LPE WS₂ dispersion samples used in this study were prepared as shown in Figure 1. The liquid-suspended WS₂ nanosheets are generated with the aid of dip sonication and stabilized against reaggregation by the surfactant sodium cholate in water. A size selection process is followed since the as-produced dispersion is highly polydisperse displaying a low monolayer content. Size selection is achieved by liquid cascade centrifugation (LCC) with subsequently increasing rotational speeds.²⁷ Heavier and multilayer nanosheets are removed in each step of the LCC process, resulting in more and more monolayer-enriched supernatants. Two size-selected nanosheet distributions are collected as sediments after 10k g and 30k g centrifugation, hereafter labelled as 5-10k g WS₂/H₂O sample and 10-30k g WS₂/H₂O sample, respectively. Isopropyl alcohol (IPA) is also known to give stable dispersions, however monolayer enrichment has not yet been demonstrated. Hence, a 10-30k g WS₂/IPA sample is also prepared in comparison by replacing the water/surfactant in the 10-30k g WS₂/H₂O sample with IPA through a centrifugation procedure. The monolayers obtained in this way are around 50 nm as characterized by transmission electron microscopy (TEM) (Figure S1a), which is similar to what was obtained from previous work.²⁰ Since mechanical exfoliation renders high quality TMD monolayers, ME WS₂ samples are also prepared as reference to LPE WS₂ samples. Large monolayer WS₂ samples (~ 200 μm) prepared on quartz substrates with mechanical exfoliation are identified by optical microscopy (Figure S1b). As shown in Figure S1c, both LPE and ME WS₂ samples on Si/SiO₂ substrates are characterized by Raman spectroscopy (excitation wavelength 532 nm), confirming the monolayer with characteristic Raman modes of monolayer WS₂ (e.g., the 2LA(M) at 354 cm⁻¹)^{28,29}.

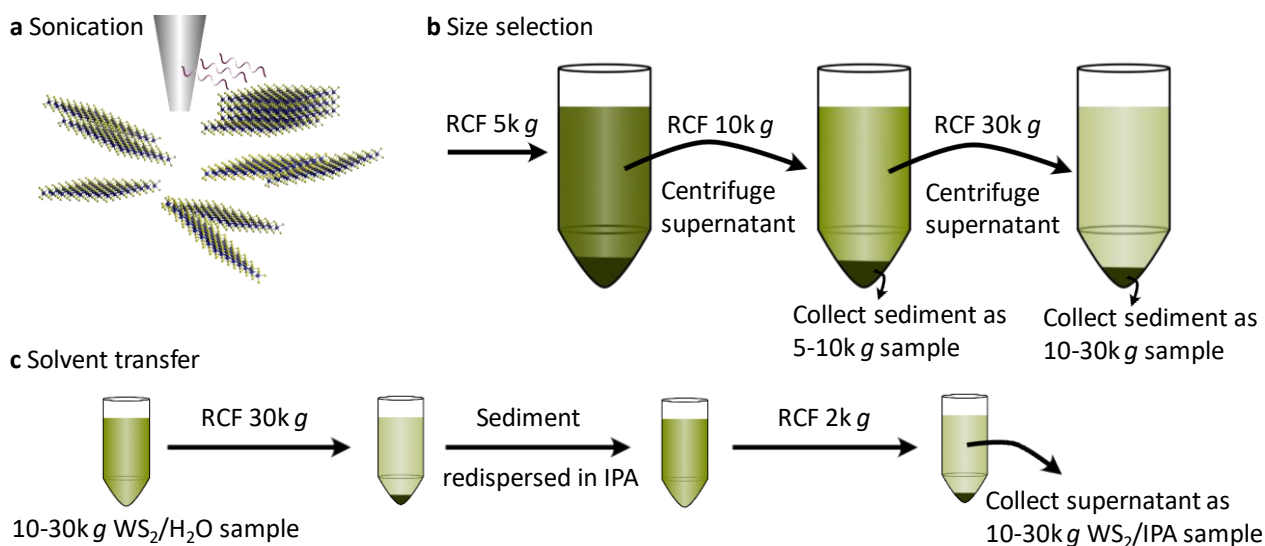


Figure 1. Illustration of liquid exfoliation, size selection and solvent transfer. **a** Schematic of the tip sonication. **b** Schematic of the liquid cascade centrifugation. Relative centrifugal forces of (RCF) 5k g, 10k g, and 30k g are used. The supernatant after each step is transferred to another centrifugation at higher centrifugal acceleration, while the sediments are collected. **c** Schematic of the dispersion solvent exchange, transferring from H₂O to IPA. 30k g RCF is used to spin down the WS₂ nanosheets as a pellet allowing for a solvent exchange. 2k g RCF is used to remove aggregated nanosheets as sediments.

The optical absorption properties of LPE 5-10k g WS₂/H₂O, 10-30k g WS₂/H₂O, and 10-30k g WS₂/IPA dispersions are characterized via UV-Vis extinction spectroscopy. The spectra depicted in Figure 2a and Figure S2a are normalized to the local minimum 290 nm, since the extinction coefficient at 290 nm is widely independent of nanosheet thickness and length.³⁰ The absorption spectra are dominated by excitonic features. The fundamental A-exciton (E_A^{ML}) for all LPE WS₂ dispersions is analysed in more detail using the second derivative of the extinction spectra (Figure 2b and Figure S2b). Due to the previously identified exponential blueshift of the A-exciton with decreasing layer number, two components are visible in the second derivative attributed to the A-exciton of the monolayer (E_A^{ML}) and the unresolvable sum of few-layers (E_A^{FL}).^{20,21,31} WS₂ dispersions in H₂O show E_A^{ML} at 2.029 eV (611 nm), while WS₂ dispersions in IPA present slightly redshifted E_A^{ML} at 2.019 eV (614 nm), which may be attributed to solvatochromism and difference of dielectric disorder.³² Since the contributions to the A-exciton absorbance of mono- and few-layer WS₂ nanosheets are differentiated, the monolayer content is estimated from the second derivative of A-exciton absorbance peak according to the previously reported method (described in SI).²⁰ There is a clear increasing monolayer volume fraction (V_f) in water dispersions with increasing RCF, which

is 17% for the 5-10k g WS₂/H₂O sample and 78% for the 10-30k g WS₂/H₂O sample, respectively. On the other hand, the 10-30k g WS₂/IPA sample shows a moderate V_f at around 35% suggesting that some aggregation occurred during the solvent transfer. In the following, we focus on the optical and photophysical properties of the monolayer-enriched LPE 10-30k g WS₂/H₂O dispersion and 10-30k g WS₂/IPA dispersion samples.

To evaluate the quality of LPE WS₂ samples, we start by comparing the steady-state PL profiles of LPE and ME WS₂ samples. The PL of ME WS₂ monolayers are measured with a confocal PL setup, while the LPE samples are measured as dispersions. As shown in Figure 2c, the PL position of ME pristine monolayer WS₂ sample (E_A^{ML} , PL) is around 1.981 eV with a full width at half maximum (FWHM) value around 44 meV, indicating the emission mainly stems from a dominating contribution of trions in the sample.¹⁰ After Li-TFSI treatment, the PL of ME monolayer WS₂ is greatly enhanced and the peak position blueshifts accompanied by a more uniform emission profile due to the suppression of trions and defects, as shown in scatter plots of the peak PL counts versus emission peak position acquired from PL spatial maps (Fig. S3). In addition, the Li-TFSI treated WS₂ sample exhibits a narrower FWHM around 10 meV. The PL Stokes shift of the ME Li-TFSI treated WS₂ sample is primarily related to strain.³³ This is in good agreement with our previous work showing that Li-TFSI treatment can minimize trap and trion states resulting in intrinsic monolayer properties.^{9,34} The PL positions of both the LPE 10-30k g WS₂/H₂O dispersion and the 10-30k g WS₂/IPA dispersion coincide with that of the monolayer A-exciton absorbance with almost no Stokes shift, suggesting a high optical quality of the samples with near intrinsic properties, Table 1. However, the monolayer enriched LPE WS₂ dispersions show extremely low PLQE, less than 0.1% as it is too low to determine accurately with our setup. The FWHM value is around 19 meV for both LPE WS₂ samples, which is wider compared to that of ME Li-TFSI treated WS₂ samples. This may be ascribed to polydispersity induced defect-related broadening of the exciton resonances.³⁵ Also, the long PL tail below the bandgap of WS₂ in the LPE 10-30k g WS₂/IPA dispersion is attributed to the larger portion of few layers caused by aggregation.

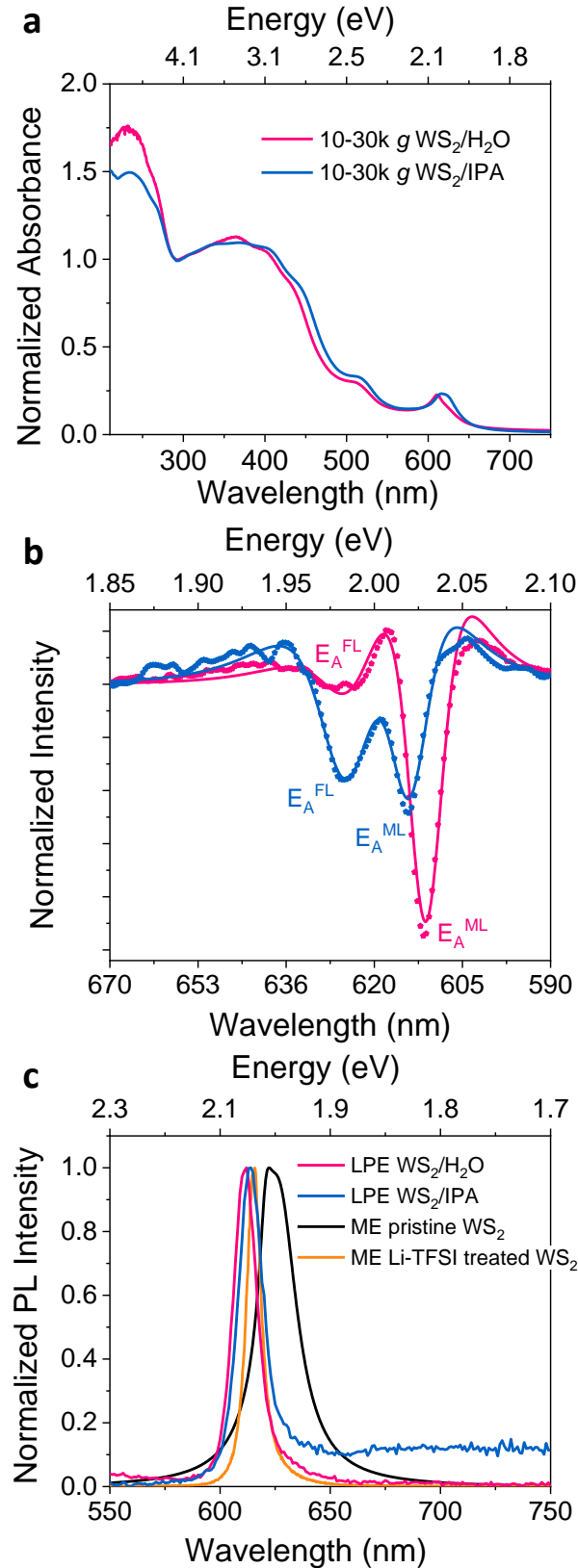


Figure 2. **a** Extinction spectra of the 10-30k g WS₂/H₂O and 10-30k g WS₂/IPA dispersion samples (normalized to 290 nm). **b** Second derivatives of the A-exciton obtained after smoothing the spectrum with the Lowess method. The spectra are fitted to the second derivative of two Lorentzians (described

in the SI). The positions of monolayer A-exciton (E_A^{ML}) and few-layer A-exciton (E_A^{FL}) are marked in the figure. **c** Normalized PL spectra of the liquid-exfoliated 10-30k g $\text{WS}_2/\text{H}_2\text{O}$ and 10-30k g WS_2/IPA dispersion samples as well as mechanically exfoliated pristine and Li-TFSI treated WS_2 samples.

Table 1. Summary of monolayer volume fraction (V_f), the position of monolayer A-exciton peak (E_A^{ML}), center and full width at half-maximum (FWHM) of PL spectra, as well as the position and average exciton lifetime $\langle\tau\rangle$ of A-exciton ground state bleach (GSB) from pump-probe measurements.

Sample	ML V_f (%)	E_A^{ML} (Abs, eV)	E_A^{ML} (PL, eV)	FWHM (PL, meV)	E_A^{ML} (GSB, eV)	$\langle\tau\rangle$ (A_{ML} - exciton GSB, ps)	$\langle\tau\rangle$ (A_{FL} - exciton GSB, ps)
LPE 10-30k g $\text{WS}_2/\text{H}_2\text{O}$	78	2.029	2.029	19	2.029	481	325
LPE 10-30k g WS_2/IPA	35	2.019	2.019	19	2.019	231	759
ME pristine WS_2	/	/	1.981	44	2.006	6	/
ME Li-TFSI treated WS_2	/	/	2.013	10	2.013	90	/

In order to investigate the reason for the low PLQE of LPE WS_2 dispersions, we conducted ultrafast pump-probe spectroscopy to explore the exciton dynamics of the LPE WS_2 dispersions and the ME WS_2 monolayer samples. Upon excitation, the state filling of the A-exciton leads to a reduction in the ground-state absorption, which is referred to as the A-exciton ground-state bleach (GSB). We record the differential transmission ($\Delta T/T$) of a white light probe beam as a function of time after photoexcitation by a pulsed laser. The full pump-probe spectra of the LPE 10-30k g $\text{WS}_2/\text{H}_2\text{O}$ dispersion, the WS_2/IPA dispersion, the ME pristine WS_2 , and the Li-TFSI treated WS_2 samples excited at around the A-exciton resonance 610 nm (2.033 eV) with 2.63 nJ/pulse are shown in Figure S4. Dynamic screening of Coulomb interaction gives rise to either a comparatively small red-shift or blue-shift of the A-exciton resonance depending on the exciton density.^{36,37} As shown in Figure 3 and summarized in Table 1, the monolayer A-exciton GSB maximum (E_A^{ML} , GSB) is located at 611 nm (2.029 eV), 614 nm (2.019 eV) and 616 nm (2.013 eV) for the LPE $\text{WS}_2/\text{H}_2\text{O}$ dispersion, the WS_2/IPA dispersion and the ME Li-TFSI treated WS_2 sample, respectively. This coincides with E_A^{ML} (PL), confirming the PL of LPE WS_2 dispersions and ME Li-TFSI treated WS_2 sample stems from neutral exciton emission. While E_A^{ML} (GSB) is detected at 618 nm (2.006 eV) for the ME pristine WS_2 monolayer, which is redshifted compared to E_A^{ML} (PL). This is in good agreement with our interpretation that PL of the ME pristine WS_2 monolayer is dominated by trion emission. In contrast

to the ME monolayers, LPE samples also display a positive feature at around 650 – 690 nm which we assign to the few-layer A-exciton GSB (E_A^{FL} , GSB). The few-layer signal is more prominent in the LPE WS_2/IPA sample than that in the 5-10k g and 10-30k g $\text{WS}_2/\text{H}_2\text{O}$ samples (Figure S4 and S5), even though the monolayer content in the WS_2/IPA dispersion is larger than that in the 5-10k g sample. This suggests that this feature is a signature of aggregated nanosheets that is increased in content during the solvent exchange process (Detailed discussion in SI).

The normalized kinetics taken at the A_{ML} -exciton GSB and A_{FL} -exciton GSB are shown in Figure 3c and the averaged decay lifetimes ($\langle\tau\rangle$) are summarized in Table 1 while the fitting results are exhibited in Table S2. For the ME pristine monolayer WS_2 sample, photogenerated excitons decay primarily through nonradiative exciton-exciton annihilation (EEA) on a few picoseconds time scale.^{38,39} After Li-TFSI treatment, $\langle\tau\rangle$ increases to tens of picoseconds, which is ascribed to radiative recombination. On the other hand, the A_{ML} -exciton GSB and A_{FL} -exciton GSB for the LPE 10-30k g $\text{WS}_2/\text{H}_2\text{O}$ dispersions exhibit much longer lifetimes compared to ME samples. The long lived species on a timescale of nanoseconds may be due to thermal repopulation of small-sized multilayer A-excitons acting as traps. For both the LPE 10-30k g $\text{WS}_2/\text{H}_2\text{O}$ and WS_2/IPA dispersions, A_{FL} -exciton GSB rises simultaneously while A_{ML} -exciton GSB goes through a fast decay at a timescale of picoseconds. The decay of the A_{ML} -exciton GSB and the initial rise and later decay of the A_{FL} -exciton GSB are fitted simultaneously with the constraint that the initial decay constant of the A_{ML} -exciton GSB and rise of the A_{FL} -exciton GSB are the same. Satisfactory fits are obtained with three exponential decays and an additional initial exponential rise for the A_{FL} -exciton GSB decays. The concomitant rise and decay of mono and multilayer signals indicates that there is energy transfer between monolayers and multilayers in LPE WS_2 dispersions, which can be responsible for the low PLQE in high quality monolayer enriched WS_2 dispersions prepared by liquid exfoliation.

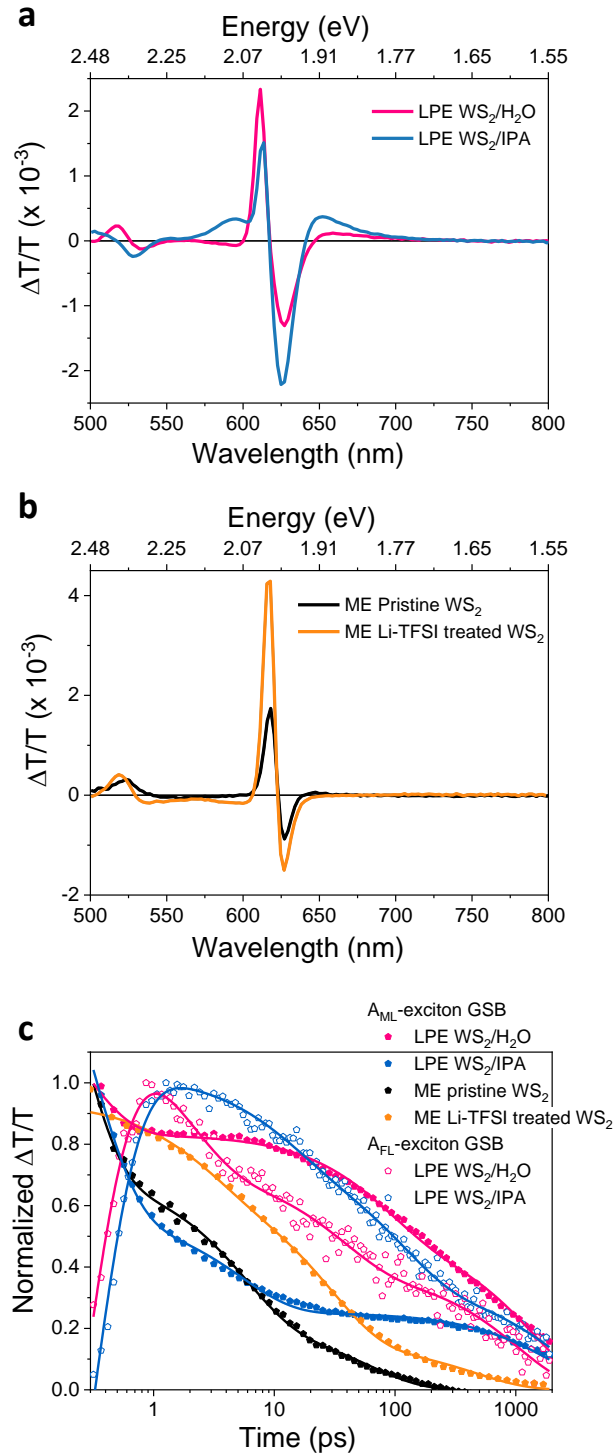


Figure 3. Ultrafast exciton dynamics. Pump-probe spectra at 10 ps time delay (610 nm excitation and 2.63 nJ/pulse) of **a** LPE 10-30k g WS₂/H₂O and LPE 10-30k g WS₂/IPA samples, and **b** ME pristine and Li-TFSI treated WS₂ monolayer samples. **c** Normalized kinetics taken at the A_{ML} -exciton GSB and A_{FL} -exciton GSB. Data are well fitted by a three exponential function (solid lines).

To test our hypothesis, we conduct further pump-probe measurement by exciting the LPE 10-30k g WS₂/IPA dispersion sample with an energy below the WS₂ bandgap, at 650 nm, to directly excite the

multilayer components and observe the exciton decay. Since the position of A_{FL} -exciton GSB redshifts with increasing layer number, all the positive features shown in Figure 4a are assigned to the A_{FL} -exciton GSB. As summarized in Table S3, simultaneous with the fast A_{FL} -exciton (~ 620 nm) decay is the growth of more aggregated A_{FL} -exciton (~ 660 nm) GSB. The further extended $\langle\tau\rangle$ at A_{FL} -exciton GSB (~ 660 nm) supports our assumption that there is energy transfer between the individual sheets in the LPE WS_2 dispersion. In this scenario, we propose that the optical quality of the LPE WS_2 can potentially be improved by reducing the energy transfer by introducing a coating on the nanosheets, for example through chemical functionalization or adsorption of bulky molecules or polymers.

In order to gain further insight into exciton dynamics of the WS_2 samples, we also analyse the photon energy dependence and pump fluence dependence of the A-exciton GSB decay feature (Figure S6-S9; Table S4-S7). A sub-picosecond decay component in the excited-state dynamics of WS_2 emerges for incident photon energies above the A-exciton resonance. This originates from a nonequilibrium population of charge carriers that form excitons as they cool, and is dependent on the photon energy.⁴¹ Nevertheless, the exciton decay for LPE WS_2 samples and ME pristine WS_2 samples are largely independent on the pump fluence (Figure S7 and S8). The fluence independent nature of the recombination indicates that it is linked to defect-assisted decay.⁴² While the $\langle\tau\rangle$ at A_{ML} -exciton GSB for ME Li-TFSI treated WS_2 samples shortens with the increase of pump fluence due to the enhanced EEA process. This suggests that there are also other reasons for the low PLQE of LPE WS_2 dispersions besides energy transfer, such as edge effects related to the small lateral dimensions of the monolayers in LPE dispersions. Hence the liquid exfoliation process needs to be further improved to produce samples suitable for practical optoelectronic application.³⁰

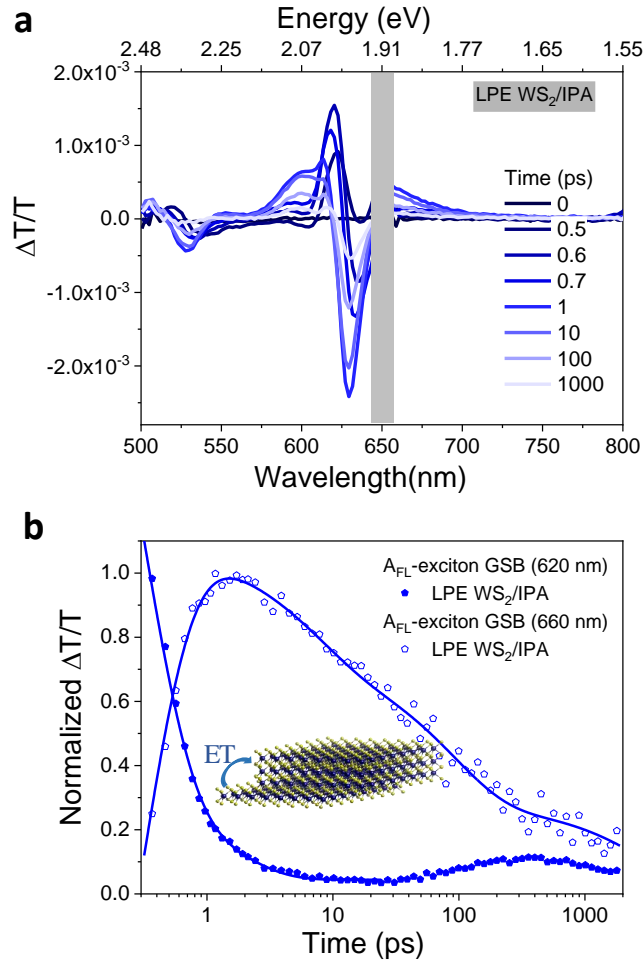


Figure 4. **a** Pump-probe spectra of the LPE 10-30k g WS₂/IPA sample at 650 nm excitation with 5.26 nJ/pulse. **b** Normalized kinetics taken at A_{ML} -exciton GSB and A_{FL} -exciton GSB, illustrating energy transfer (ET) from monolayers to multilayers. Data are well fit by three exponential decay function and an additional rise component for the A_{FL} -exciton GSB (solid lines).

In conclusion, monolayer enriched WS₂ dispersions produced by liquid phase exfoliation combined with size selection and WS₂ monolayers by mechanical exfoliation were prepared and the quality of the samples compared and investigated with respect to the optical and photophysical properties. Our results reveal that LPE monolayer-enriched WS₂ dispersions show pristine-like excitonic feature with narrow linewidth PL and minimal Stoke shift. In addition, we conduct a detailed analysis on the exciton dynamics of LPE WS₂ dispersions and ME WS₂ monolayers through pump-probe spectroscopy, and elucidate that there is an energy transfer between individual monolayer and multilayers nanosheets in the LPE WS₂ dispersions which is at least partly responsible for their low PLQE in addition to other factors such as small lateral sheet size. We also propose that a thicker coating shielding the sheets such as polymers as additional stabilizers can potentially reduce this

phenomenon. As such, the study clearly identifies anchor points for further improving the liquid exfoliation methodology to produce materials with great potential in practical optoelectronic applications.

Experimental Methods

Material

WS₂ powder (99%, 2 μm, Sigma A), surfactant sodium cholate hydrate (SC, ≥ 99%), and bis(trifluoromethane)sulfonimide lithium salt (Li-TFSI) are purchased from Sigma-Aldrich and used without purification. The bulk synthetic WS₂ crystal is purchased from 2D Semiconductors. The mechanically-exfoliated monolayer WS₂ is prepared according to the reported gold-mediated exfoliation method to ensure relatively large monolayers.⁴³

Liquid exfoliation process

WS₂ powder (30 g/L) and SC (8 g/L) are added in a glass bottle with 80 mL deionized water and the dispersion is transferred to a stainless-steel beaker for sonication. The beaker is placed in a cooled water bath with a temperature of 5 °C (maintained through a chiller). An ultrasonic replaceable tip is positioned in the dispersion ~2 cm from the bottom and the mixture is sonicated for 1 h with 60% amplitude (pulse 8 s on and 2 s off ratio), using a Sonics Vibracell VCX 500, equipped with a threaded probe. The metal beaker is covered with aluminium foil during the sonication process. After the sonication, the dispersion is centrifuged at 6000 RPM for 1.5 h at 8 °C in a Hettich Mikro 220R centrifuge, equipped with a 1016 fixed-angle rotor. The participants are removed afterwards and 2 g/L SC solution is added to the dispersion to reach 80 mL, followed by another tip sonication with same amplitude at 5 °C for 5.5 h. The first sonication step serves the purpose of removing impurities in the WS₂ powder. After the second sonication, the dispersion is transferred to centrifuge tubes for size selection by liquid cascade centrifugation.²⁰ First, the dispersions are centrifuged with relative centrifugal force (RCF) 5k g for 1 h at 8 °C. Supernatant and sediment are separated through manual pipetting. The supernatant is collected and centrifuged with the same speed for 2 h at 8 °C to remove large/thick sheets as completely as possible. Then the supernatant is centrifuged with RCF 10k g for 2 h at 8 °C. The sediment is collected and dispersed in 0.1 g/L SC solution (~ 2mL), which is referred to 5-10k g WS₂/H₂O sample. The supernatant is transferred to new centrifuge tubes for further centrifugation with RCF 30k g for 2 h at 8 °C. In the end, the supernatant is discarded, while the sediment is collected and dispersed in 0.1 g/L SC solution (~ 2mL), which is referred to 10-30k g WS₂/H₂O sample. To transfer the 10-30k g WS₂/H₂O sample from water to IPA, the dispersion is centrifuged with RCF 30k g for 1.5 h to pellet out the nanosheets as sediment and decant the water supernatant. The sediment is redispersed in IPA through 5 min bath sonication. Then the dispersion

is centrifuged with RCF 2k g for 20 min to remove the majority of aggregates. The supernatant is collected as 10-30k g WS₂/IPA sample.

Chemical treatment

The chemical treatment with Li-TFSI (0.02 M in Methanol) is carried out in ambient atmosphere. The chemical treatments are achieved by immersing the samples into concentrated solutions of the investigated chemicals for 40 mins, and blow dry with nitrogen gun afterwards.

Supporting Information

Supporting Information is available online with additional experimental details as well as additional data for optical and photophysical characterization of WS₂ samples.

Data available in University of Cambridge data repository at: link to be added during proof.

Acknowledgement

This project has received funding from the European Research Council (ERC) under the European Union's Horizon 2020 research and innovation program (**Grant Agreement No.....**). Z.L. acknowledges funding from the Swedish research council, Vetenskapsrådet 2018-06610. We acknowledge financial support from the EPSRC and the Winton Programme for the Physics of Sustainability. C. B. acknowledges support from the German research foundation (DFG) under grant agreement Emmy-Noether, BA4856/2-1 and Jana Zaumseil for the access to the infrastructure at the Chair of Applied Physical Chemistry.

Reference

1. Zhang, H., Chhowalla, M. & Liu, Z. 2D nanomaterials: Graphene and transition metal dichalcogenides. *Chem. Soc. Rev.* **47**, 3015–3017 (2018).
2. Tan, C. *et al.* Recent Advances in Ultrathin Two-Dimensional Nanomaterials. *Chem. Rev.* **117**, 6225–6331 (2017).
3. Wang, J., Verzhbitskiy, I. & Eda, G. Electroluminescent Devices Based on 2D Semiconducting Transition Metal Dichalcogenides. *Adv. Mater.* **30**, 1–14 (2018).
4. Zhang, Y. J. *et al.* Enhanced intrinsic photovoltaic effect in tungsten disulfide nanotubes. *Nature* **570**, 349–353 (2019).
5. Kang, S. *et al.* 2D semiconducting materials for electronic and optoelectronic applications: Potential and challenge. *2D Mater.* **7**, (2020).
6. Mak, K. F. & Shan, J. Photonics and optoelectronics of 2D semiconductor transition metal

- dichalcogenides. *Nat. Photonics* **10**, 216–226 (2016).
7. Samadi, M. *et al.* Group 6 transition metal dichalcogenide nanomaterials: Synthesis, applications and future perspectives. *Nanoscale Horizons* **3**, 90–204 (2018).
 8. Coleman, J. N. *et al.* Two-dimensional nanosheets produced by liquid exfoliation of layered materials. *Science* (80-.). **331**, 568–571 (2011).
 9. Bretscher, H. M., Li, Z., Xiao, J., Qiu, D. Y. & Refaely-abramson, S. The bright side of defects in MoS₂ and WS₂ and a generalizable chemical treatment protocol for defect passivation. *Arxiv:2002.03956* (2020).
 10. Tanoh, A. O. A. *et al.* Enhancing Photoluminescence and Mobilities in WS₂ Monolayers with Oleic Acid Ligands. *Nano Lett.* **19**, (2019).
 11. Witomska, S., Leydecker, T., Ciesielski, A. & Samorì, P. Production and Patterning of Liquid Phase–Exfoliated 2D Sheets for Applications in Optoelectronics. *Adv. Funct. Mater.* **29**, 1–23 (2019).
 12. Cai, X., Luo, Y., Liu, B. & Cheng, H. M. Preparation of 2D material dispersions and their applications. *Chem. Soc. Rev.* **47**, 6224–6266 (2018).
 13. Hernandez, Y. *et al.* High-yield production of graphene by liquid-phase exfoliation of graphite. *Nat. Nanotechnol.* **3**, 563–568 (2008).
 14. Backes, C. *et al.* Equipartition of Energy Defines the Size-Thickness Relationship in Liquid-Exfoliated Nanosheets. *ACS Nano* (2019) doi:10.1021/acsnano.9b02234.
 15. Coleman, J. N. Liquid-phase exfoliation of nanotubes and graphene. *Adv. Funct. Mater.* **19**, 3680–3695 (2009).
 16. Hu, G. *et al.* Functional inks and printing of two-dimensional materials. *Chem. Soc. Rev.* **47**, 3265–3300 (2018).
 17. Bonaccorso, F., Bartolotta, A., Coleman, J. N. & Backes, C. 2D-Crystal-Based Functional Inks. *Adv. Mater.* **28**, 6136–6166 (2016).
 18. Zhang, Q., Mei, L., Cao, X., Tang, Y. & Zeng, Z. Intercalation and exfoliation chemistries of transition metal dichalcogenides. *J. Mater. Chem. A* **8**, 15417–15444 (2020).
 19. Backes, C. *et al.* Production and processing of graphene and related materials. *2D Mater.* **7**, (2020).
 20. Backes, C. *et al.* Production of highly monolayer enriched dispersions of liquid-exfoliated nanosheets by liquid cascade centrifugation. *ACS Nano* **10**, 1589–1601 (2016).
 21. Synnatschke, K. *et al.* Length- And Thickness-Dependent Optical Response of Liquid-Exfoliated Transition Metal Dichalcogenides. *Chem. Mater.* **31**, 10049–10062 (2019).
 22. Kłopotowski *et al.* Revealing the nature of excitons in liquid exfoliated monolayer tungsten

- disulphide. *Nanotechnology* **27**, 1–9 (2016).
23. Vega-Mayoral, V. *et al.* Charge trapping and coalescence dynamics in few layer MoS₂. *2D Mater.* **5**, (2018).
 24. Wibmer, L., Lages, S., Unruh, T. & Guldi, D. M. Excitons and Trions in One-Photon- and Two-Photon-Excited MoS₂: A Study in Dispersions. *Adv. Mater.* **30**, 1–10 (2018).
 25. Schiettecatte, P., Geiregat, P. & Hens, Z. Ultrafast Carrier Dynamics in Few-Layer Colloidal Molybdenum Disulfide Probed by Broadband Transient Absorption Spectroscopy. *J. Phys. Chem. C* **123**, 10571–10577 (2019).
 26. Zhou, P. *et al.* Ultrafast carrier dynamics in colloidal WS₂ nanosheets obtained through a hot injection synthesis. *J. Chem. Phys.* **151**, (2019).
 27. Backes, C. *et al.* Guidelines for exfoliation, characterization and processing of layered materials produced by liquid exfoliation. *Chem. Mater.* **29**, 243–255 (2017).
 28. Zhang, X. *et al.* Phonon and Raman scattering of two-dimensional transition metal dichalcogenides from monolayer, multilayer to bulk material. *Chem. Soc. Rev.* **44**, 2757–2785 (2015).
 29. Berkdemir, A. *et al.* Identification of individual and few layers of WS₂ using Raman Spectroscopy. *Sci. Rep.* **3**, 1–8 (2013).
 30. Backes, C. *et al.* Edge and confinement effects allow in situ measurement of size and thickness of liquid-exfoliated nanosheets. *Nat. Commun.* **5**, 1–10 (2014).
 31. Niu, Y. *et al.* Thickness-dependent differential reflectance spectra of monolayer and few-layer MoS₂, MoSe₂, WS₂ and WSe₂. *Nanomaterials* **8**, (2018).
 32. Raja, A. *et al.* Dielectric disorder in two-dimensional materials. *Nat. Nanotechnol.* **14**, 832–837 (2019).
 33. Kolesnichenko, P. V. *et al.* Disentangling the effects of doping, strain and disorder in monolayer WS₂ by optical spectroscopy. *2D Mater.* **7**, (2020).
 34. Li, Z. *et al.* Mechanistic insight to the chemical treatments of monolayer transition metal disulfides for photoluminescence enhancement. *arXiv* (2020).
 35. Selig, M. *et al.* Excitonic linewidth and coherence lifetime in monolayer transition metal dichalcogenides. *Nat. Commun.* **7**, (2016).
 36. Sie, E. J. *et al.* Observation of Exciton Redshift-Blueshift Crossover in Monolayer WS₂. *Nano Lett.* **17**, 4210–4216 (2017).
 37. Ugeda, M. M. *et al.* Giant bandgap renormalization and excitonic effects in a monolayer transition metal dichalcogenide semiconductor. *Nat. Mater.* **13**, 1091–1095 (2014).
 38. Jiang, T., Chen, R., Zheng, X., Xu, Z. & Tang, Y. Photo-induced excitonic structure

- renormalization and broadband absorption in monolayer tungsten disulphide. *Opt. Express* **26**, 859 (2018).
39. Yuan, L., Wang, T., Zhu, T., Zhou, M. & Huang, L. Exciton Dynamics, Transport, and Annihilation in Atomically Thin Two-Dimensional Semiconductors. *J. Phys. Chem. Lett.* **8**, 3371–3379 (2017).
 40. Tao, H. *et al.* Scalable exfoliation and dispersion of two-dimensional materials-an update. *Phys. Chem. Chem. Phys.* **19**, 921–960 (2017).
 41. Cunningham, P. D., Hanbicki, A. T., McCreary, K. M. & Jonker, B. T. Photoinduced Bandgap Renormalization and Exciton Binding Energy Reduction in WS₂. *ACS Nano* **11**, 12601–12608 (2017).
 42. Yu, Y. *et al.* Fundamental limits of exciton-exciton annihilation for light emission in transition metal dichalcogenide monolayers. *Phys. Rev. B* **93**, 2–6 (2016).
 43. Desai, S. B. *et al.* Gold-Mediated Exfoliation of Ultralarge Optoelectronically-Perfect Monolayers. *Adv. Mater.* **28**, 4053–4058 (2016).

Supporting Information

Photophysical Comparison of Liquid and Mechanically Exfoliated WS₂ Monolayers

Zhaojun Li^{1,2}, Farnia Rashvand³, Hope Bretscher¹, Beata M. Szydłowska³, James Xiao¹, Claudia Backes^{3,4}, Akshay Rao^{1*}

¹Cavendish Laboratory, University of Cambridge, JJ Thomson Avenue, CB3 0HE, Cambridge, United Kingdom

²Molecular and Condensed Matter Physics, Department of Physics and Astronomy, Uppsala University, 75120 Uppsala, Sweden

³Institute for Physical Chemistry, Ruprecht-Karls-Universität Heidelberg, Im Neuenheimer Feld 253, 69120 Heidelberg, Germany

⁴Current address: Physical Chemistry of Nanomaterials, University of Kassel, Heinrich-Plett-Str.40, D-34132 Kassel, Germany

*Corresponding author

Contact e-mail: ar525@cam.ac.uk

Contents

1. Experimental Details	2
2. Calculation of Monolayer Content	3
3. Material characterization	4
4. Optical properties of LPE WS ₂ dispersions and ME WS ₂ samples.....	5
5. Additional Pump-probe data on WS ₂ samples.....	6
6. Reference	14

1. Experimental Details

Si/SiO₂ substrates with 90 nm oxide layer were used for microscope steady-state photoluminescence (PL) and Raman spectroscopy. Quartz substrates were used for ultrafast pump-probe measurement. The samples were encapsulated for ultrafast pump-probe measurements, and other measurements are carried out on samples without encapsulation.

Transmission electron microscopy (TEM) was performed using a FEI Tecnai F20 at 200kV accelerating voltage. 10-30k g WS₂/H₂O dispersion sample was transferred onto 200-mesh Cu grids (Agar AGS160). The optical microscopy was measured using Olympus BX60 optical microscope with 405 nm laser. Samples were placed on an X-Y piezo stage of the microscope and the signal is collected in reflection mode with the 50× objective. The Raman spectroscopy was carried out on a Renishaw inVia Raman confocal microscope with a 532 nm excitation laser in air under ambient condition. The Raman emission was collected by a 20× long working distance objective lens in streamline mode and dispersed by a 1800 l/mm grating with 1% of the laser power (< 10 μW). The spectrometer was calibrated to a silicon reference sample prior to the measurement to correct for the instrument response.

UV-Vis measurement was performed using a Shimadzu UV-3600 Plus spectrometer to measure the extinction spectra of the LPE WS₂ dispersions in transmission mode in quartz cuvettes with 1 nm increments. Steady-state PL measurement were carried out using a temperature and current-controlled 405 nm laser diode (Thorlabs). The incident beam was attenuated as desired and focused onto the sample while PL from the sample was collected and focused into an Andor Kymera 328i Spectrometer and spectra recorded using a Si-CCd (Andor iDus 420).

The microscope steady-state PL measurement was carried out using a WITec alpha 300 s setup as has been described previously.¹ Importantly, a 405 nm continuous wave laser (Coherent CUBE) was used as the excitation source. A long pass filter with a cutoff wavelength of 450 nm was fitted before signal collection to block excitation scatter. The light was coupled with an optical fiber to the microscope and focused using a 20× Olympus lens. Samples were placed on an X-Y piezo stage of the microscope. The PL signal was collected in reflection mode with the same 20× objective and

detected using a Princeton Instruments SP-2300i spectrometer fitted with an Andor iDus 401 CCD detector. The PL was measured at 405 nm excitation with a fluence of 15 W cm⁻².

The ultrafast pump-probe setup has been described previously.² A Light Conversion PHAROS laser system with 400 μJ per pulse at 1030 nm with a repetition rate of 38 kHz is split in two, one part is used to generate the continuum probe light and the second part is used in an Collinear Optical Parametric Amplifier (Orpheus, Light Conversion) to generate the pump source at the desired wavelength. The probe pulse is delayed up to 2 ns with a mechanical delay-stage (Newport). A mechanical chopper (Thorlabs) is used to create an on-off pump-probe pulse series. A silicon line scan camera (JAI SW-2000M-CL-80) fitted onto a visible spectrograph (Andor Solis, Shamrock) is used to record the transmitted probe light.

2. Calculation of Monolayer Content

The monolayer volume fraction (V_f) can be extracted from the extinction spectra of the dispersion according to the previously reported method.³ The A-exciton extinction is first deconvoluted into components of monolayered and multi-layered WS₂ with differentiation after smoothing the spectra by the Lowess method (10-15 points). The smoothing function suppresses spectral noise well without changing peak shapes. In the simplest form, a Lorentzian line can be described by

$$L(E) = \frac{h}{\left[1 + \left(\frac{E - E_0}{w/2}\right)^2\right]} \quad (S1)$$

Where h represents the height, E_0 the center and w the full width half maximum (FWHM). Differentiating twice with respect to E gives

$$\frac{d^2L(E)}{dE^2} = -\frac{8h}{w^2} \left[\frac{1 - 3\left(\frac{E - E_0}{w/2}\right)^2}{\left(1 + \left(\frac{E - E_0}{w/2}\right)^2\right)^3} \right] \quad (S2)$$

The obtained spectrum of the second derivative is then fitted to the sum of the second derivative of two Lorentzian functions giving E , w and h of the monolayer and few-layer WS₂. The area under the monolayer (ML) A-exciton extinction peak should scale with the monolayer content in the dispersion. As the area under any Lorentzian is proportional to $h \times w$, a metric S_A which scales with the V_f can be calculated as the equation:

$$S_A = \frac{h_{ML}w_{ML}}{h_{ML}w_{ML} + h_{FL}w_{FL}} \quad (S3)$$

V_f is then calculated as:³

$$V_f = (1.25 \pm 0.08)S_A \quad (S4)$$

3. Material characterization

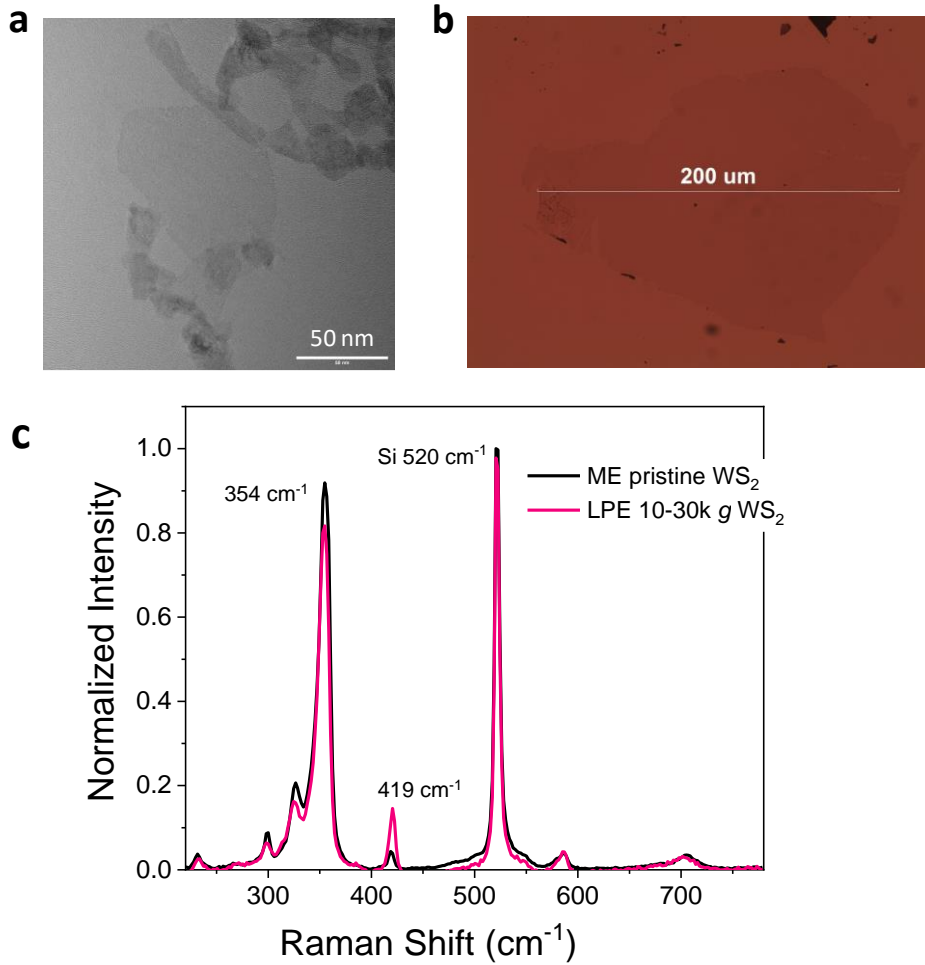


Figure S1. Characterization of liquid exfoliated and mechanically exfoliated WS₂ samples. **a** TEM image of liquid phase exfoliated 10-30k g WS₂ sample. **b** Optical microscope image of mechanically exfoliated WS₂ sample on quartz substrate. **c** Raman spectroscopy of liquid phase exfoliated and mechanically exfoliated WS₂ samples on Si/SiO₂ substrate confirming the monolayer.

4. Optical properties of LPE WS₂ dispersions and ME WS₂ samples

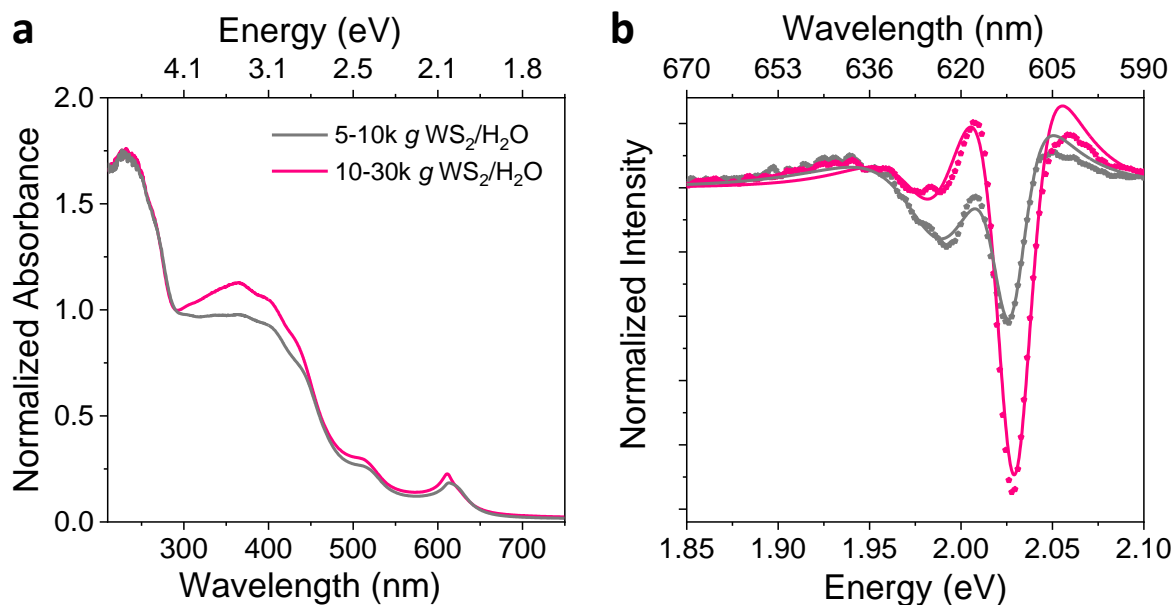


Figure S2. **a** Extinction spectra normalized to 290 nm of the 5-10k g and 10-30k g WS₂/H₂O samples. **b** Second derivatives of the A-exciton obtained after smoothing the spectrum with the Lowess method. The spectra are fitted to the second derivative of two Lorentzians (solid lines).

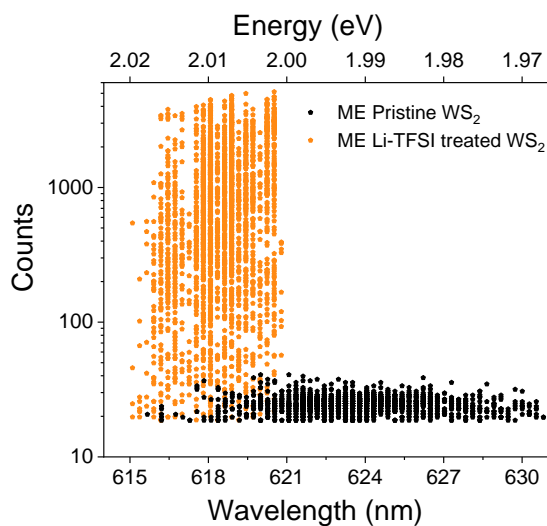


Figure S3. PL scatter plots of spectral position of the peak emission as well as peak pristine and Li-TFSI-treated monolayer WS₂ PL counts extracted from PL maps of WS₂ monolayer on Si-SiO₂ (90 nm) substrate.

5. Additional Pump-probe data on WS₂ samples

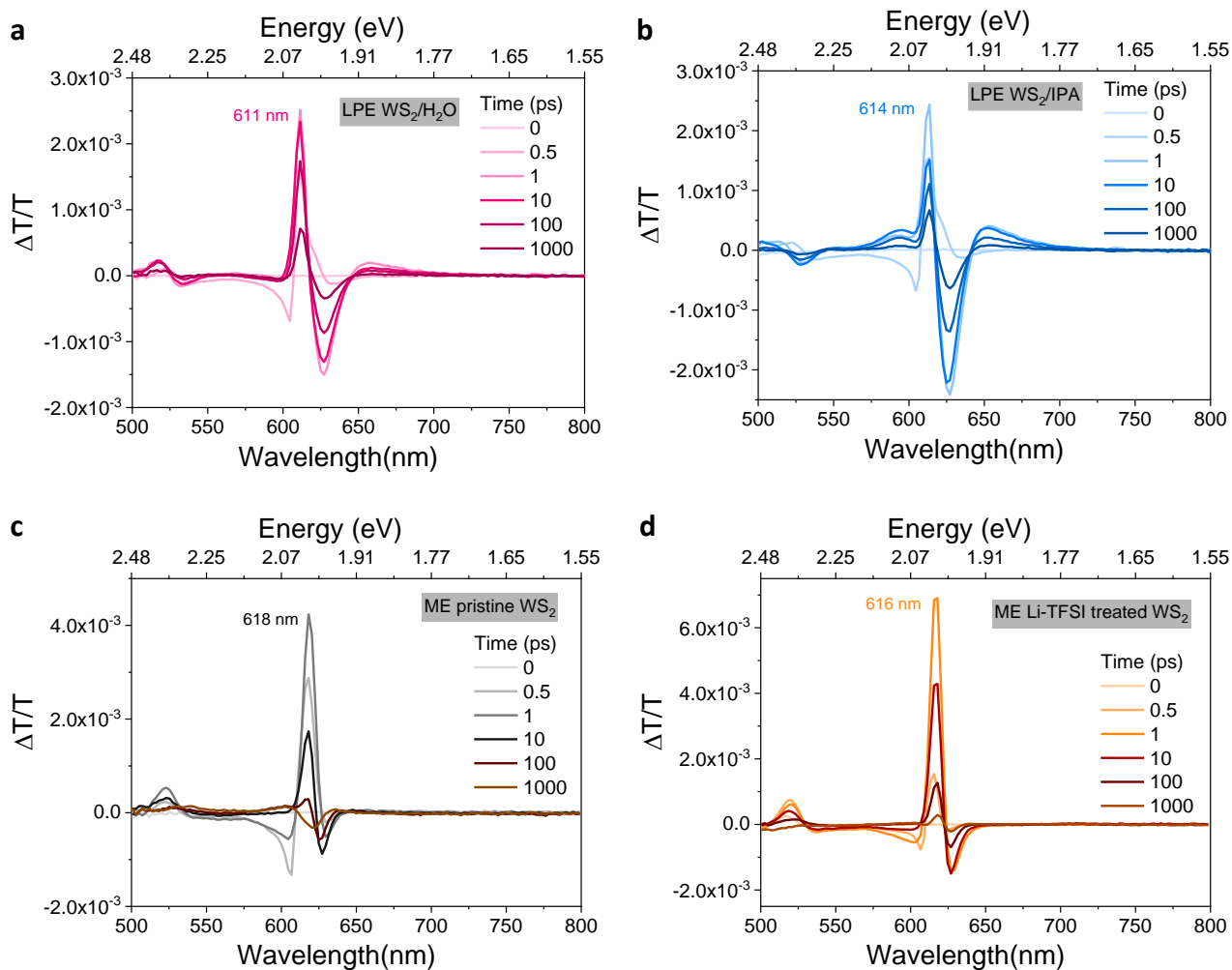


Figure S4. Pump-probe spectra (excited at 610 nm, 2.63 nJ/pulse) of **a** liquid exfoliated 10-30k g WS₂/H₂O, **b** liquid phase exfoliated 10-30k g WS₂/IPA, **c** mechanically exfoliated pristine WS₂ monolayer sample, and **d** mechanically exfoliated Li-TFSI treated WS₂ monolayer sample.

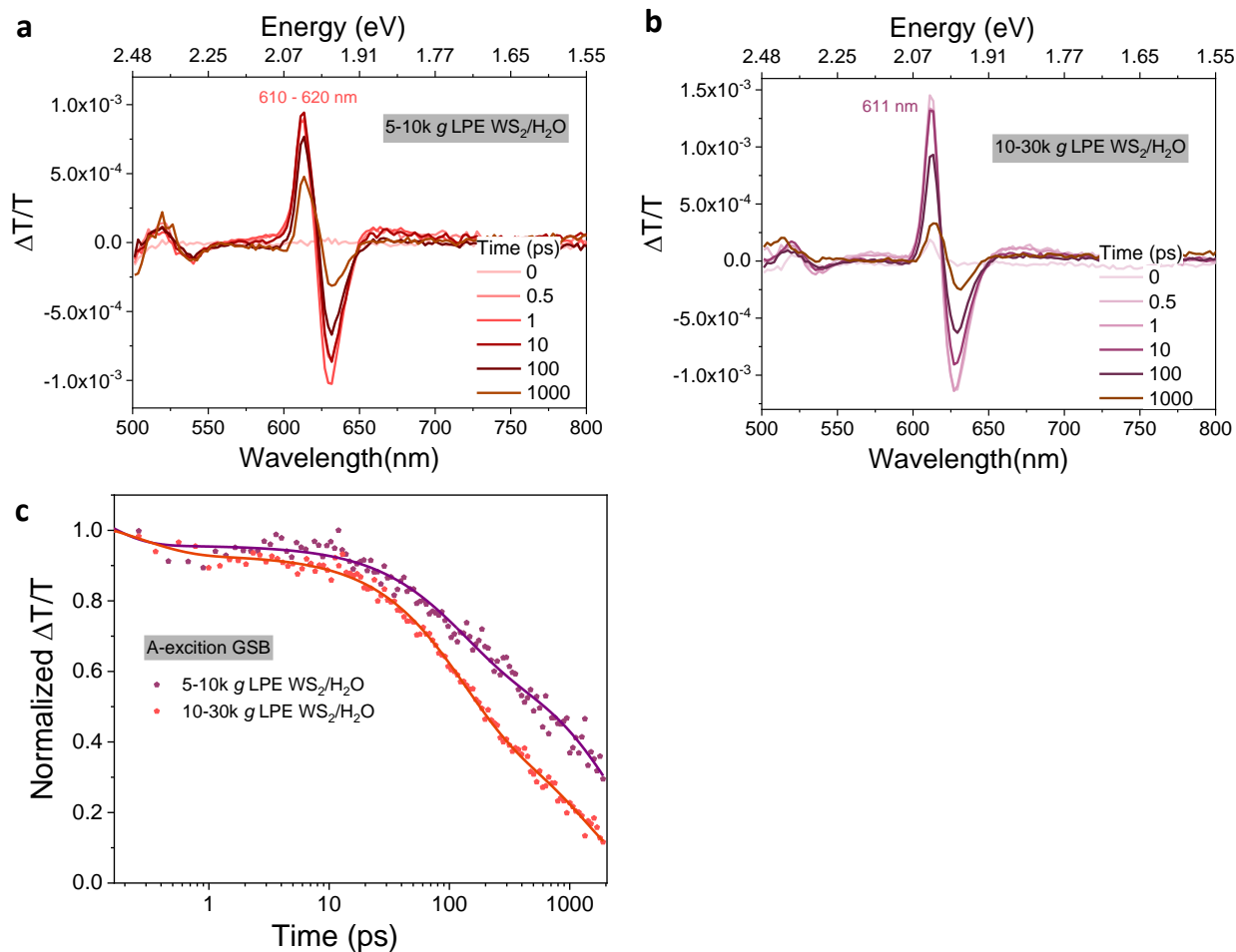


Figure S5. Pump-probe spectra (excited at 500 nm, 0.53 nJ/pulse) of **a** liquid phase exfoliated 5-10k g WS₂/H₂O sample, **b** liquid phase exfoliated 10-30k g WS₂/ H₂O sample. **c** Normalized kinetics of A-exciton GSB of both samples.

Table S1. Fitting results of the rates for LPE 10-30k g WS₂/IPA sample at 500 nm excitation with 0.53 nJ/pulse in pump-probe measurement.

Sample	A ₁	τ ₁ (ps)	A ₂	τ ₂ (ps)	A ₃	τ ₃ (ps)	<τ> (ps)
LPE 5-10k g WS ₂ /H ₂ O AML-exciton GSB (~611 nm)	0.25	0.10	0.32	114	0.63	2591	1391
LPE 10-30k g WS ₂ / H ₂ O A-exciton GSB (610~620 nm)	0.13	0.26	0.48	116	0.45	1419	655

Compared to the LPE 10-30k g WS₂/IPA dispersion, both 5-10k g and 10-30k g WS₂/H₂O show less positive features in the 650 – 680 nm region in the pump-probe spectra, suggesting the fraction of

multilayers are less than that of WS₂/IPA samples (Figure S4 and S5). This is understandable for 10-30k g WS₂/H₂O sample since the V_f is really high, around 78%, however, the V_f in 5-10k g WS₂/H₂O sample is quite low (~ 15%). On the other hand, compared to the narrow linewidth of A_{ML}-exciton GSB for both LPE 10-30k g WS₂/H₂O and WS₂/IPA, the 5-10k g sample shows wider linewidth and even peak splitting in the longer time delay stage. In addition, the A_{ML}-exciton GSB of the 5-10k g sample decays slower than that LPE 10-30k g WS₂/H₂O (Figure S5 c and Table S1), indicating there are multilayers which are not distinguishable from monolayer in 5-10k g sample and possible energy transfer between them. Therefore, we assume the multilayers existing in 5-10k g WS₂/H₂O and 10-30k g WS₂/IPA are different. There are more double or triple layers in 5-10k g WS₂/H₂O sample which is removed with high centrifugation speed, while there are more aggregated multilayers in 10-30k g WS₂/IPA sample due to the reaggregation occurring during the solvent exchange process.

Table S2. Fitting results for the rates at 610 nm excitation with 2.63 nJ/pulse in pump-probe measurement.

Sample	A ₁	τ ₁ (ps)	A ₂	τ ₂ (ps)	A ₃	τ ₃ (ps)	A ₄	τ ₄ (ps)	<τ> (ps)
LPE 10-30k g WS ₂ /H ₂ O A _{ML} -exciton GSB	0.65	0.23	0.34	82	0.49	1396	/	/	481
LPE 10-30k g WS ₂ /H ₂ O A _{FL} -exciton GSB	-3.6	0.23	0.54	1.8	0.33	35	0.38	1034	360
LPE 10-30k g WS ₂ /IPA A _{ML} -exciton GSB	1.64	0.26	0.32	5.3	0.25	2032	/	/	231
LPE 10-30k g WS ₂ /IPA A _{FL} -exciton GSB	-3.6	0.26	0.26	12	0.43	111	0.34	2151	759
ME pristine WS ₂ A _{ML} -exciton GSB	0.74	0.18	0.18	5.5	0.08	63	/	/	6
ME Li-TFSI treated WS ₂ A _{ML} -exciton GSB	0.29	2.7	0.55	29	0.16	466	/	/	90

Table S3. Fitting results for the rates for LPE 10-30k g WS₂/IPA sample at 650 nm excitation with 5.26 nJ/pulse in pump-probe measurement.

Sample	A_1	τ_1 (ps)	A_2	τ_2 (ps)	A_3	τ_3 (ps)	A_4	τ_4 (ps)	$\langle \tau \rangle$ (ps)
LPE 10-30k g WS ₂ /IPA A _{FL} -exciton GSB (~620 nm)	2.64	0.28	0.27	1.5	0.04	367	/	/	6
LPE 10-30k g WS ₂ /IPA A _{FL} -exciton GSB (~660 nm)	-2.95	0.28	0.35	6.7	0.45	89	0.27	3156	836

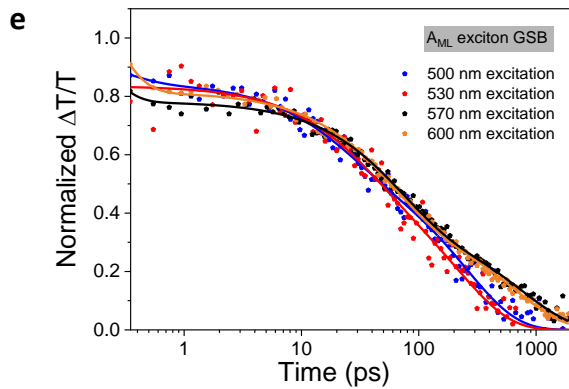
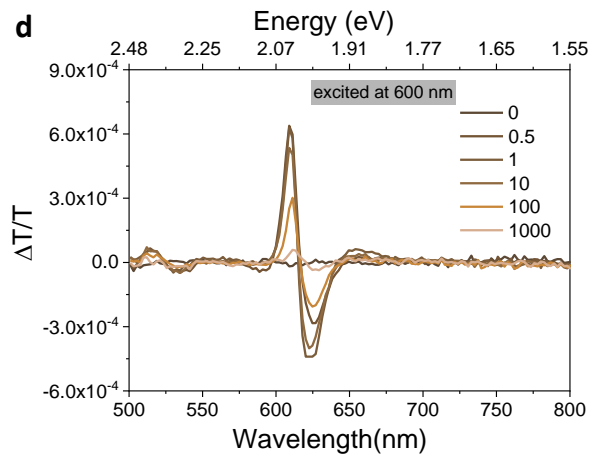
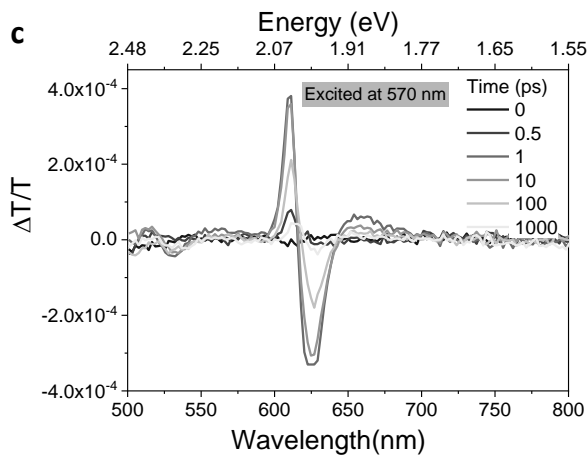
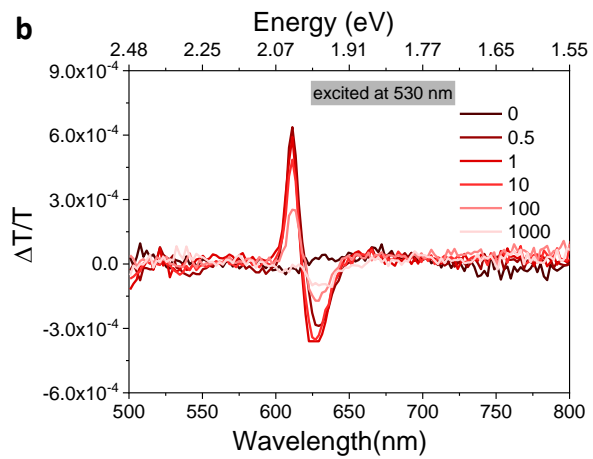
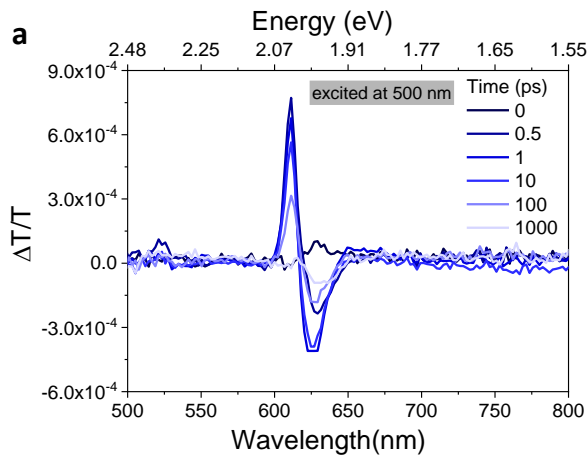


Figure S6. Photon energy dependence of A-exciton resonance with 0.53 nJ/pulse in pump-probe measurements. **a** pump-probe data of the 10-30k g WS₂/H₂O sample excited at **a** 500 nm, **b** 530 nm, **c** 570 nm, and **d** 600 nm. **e** Normalized kinetics of A_{ML}-exciton GSB of all samples.

Table S4. Fitting results for the rates of the 10-30k g WS₂/H₂O sample with 0.53 nJ/pulse in pump-probe measurement.

Sample	A ₁	τ ₁ (ps)	A ₂	τ ₂ (ps)	A ₃	τ ₃ (ps)	<τ> (ps)
500 nm excitation	0.16	0.2	0.28	21.7	0.57	254	149
530 nm excitation	0.15	0.07	0.29	30.5	0.54	223	132
570 nm excitation	1.2	0.1	0.42	65.2	0.36	763	153
600 nm excitation	1.4	0.1	0.44	65.1	0.38	655	125

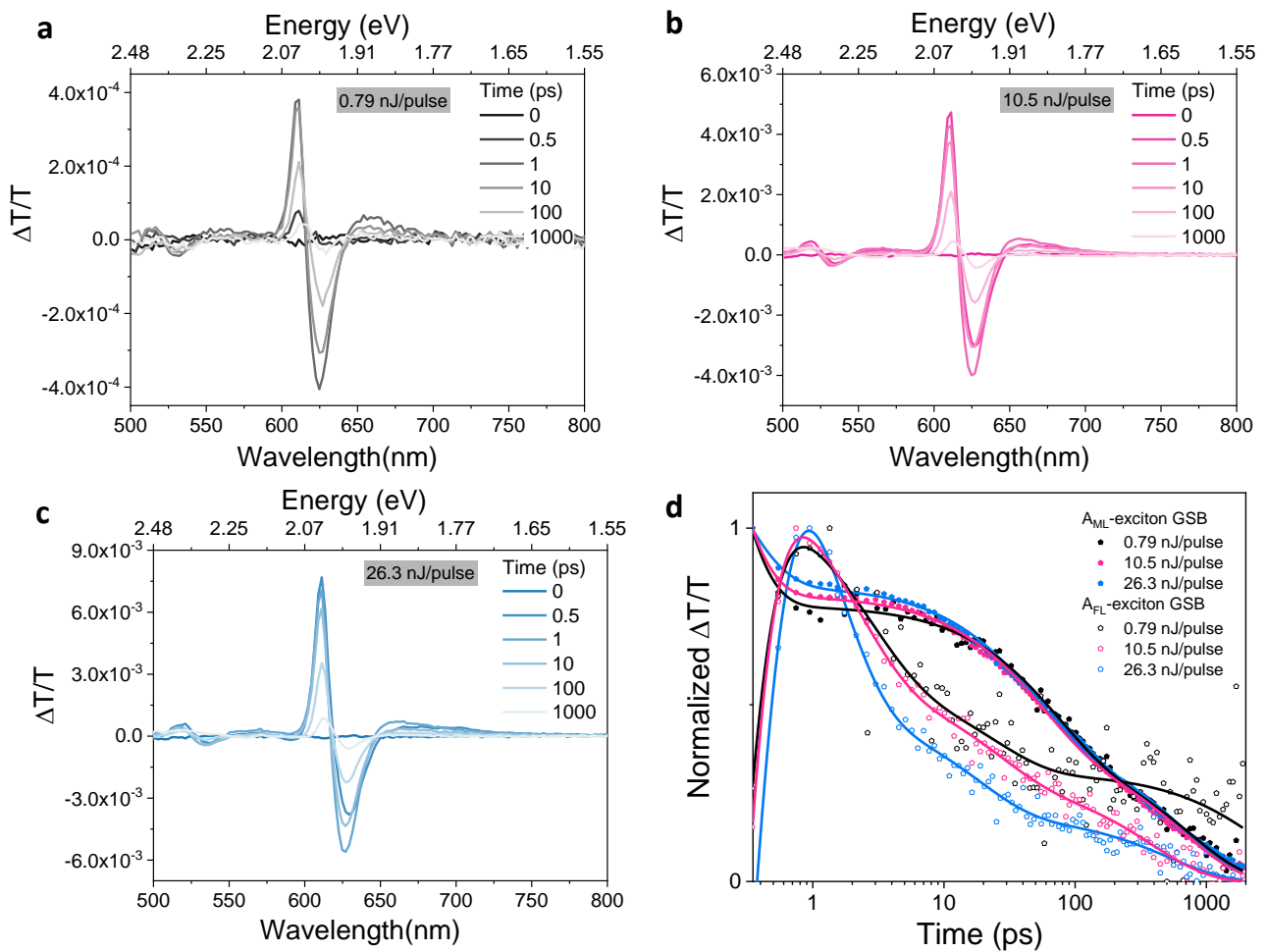


Figure S7. Fluence dependence of A-exciton resonance (excited at 570 nm). **a** pump-probe data of the 10-30k g WS₂/H₂O sample excited with **a** 0.79 nJ/pulse, **b** 10.5 nJ/pulse, and **c** 26.3 nJ/pulse. **d** Normalized kinetics of A_{ML}-exciton GSB and A_{FL}-exciton GSB of all samples.

Table S5. Fitting results for the rates at 570 nm excitation of the 10-30k g WS₂/H₂O sample in pump-probe measurement.

Sample	A ₁	τ_1 (ps)	A ₂	τ_2 (ps)	A ₃	τ_3 (ps)	A ₄	τ_4 (ps)	$\langle\tau\rangle$ (ps)
0.79 nJ/pulse A _{ML} -exciton GSB	2.1	0.14	0.42	66	0.36	766	/	/	106
0.79 nJ/pulse A _{FL} -exciton GSB	-8.9	0.14	0.57	2.6	0.27	24	0.31	2692	733
10.5 nJ/pulse A _{ML} -exciton GSB	1.97	0.15	0.43	51	0.38	667	/	/	99
10.5 nJ/pulse A _{FL} -exciton GSB	-10.2	0.15	0.69	2.0	0.28	24	0.28	386	93
26.3 nJ/pulse A _{ML} -exciton GSB	0.8	0.2	0.44	47	0.4	685	/	/	180
26.3 nJ/pulse A _{FL} -exciton GSB	-8.29	0.2	1.32	1.3	0.3	17.6	0.19	518	58

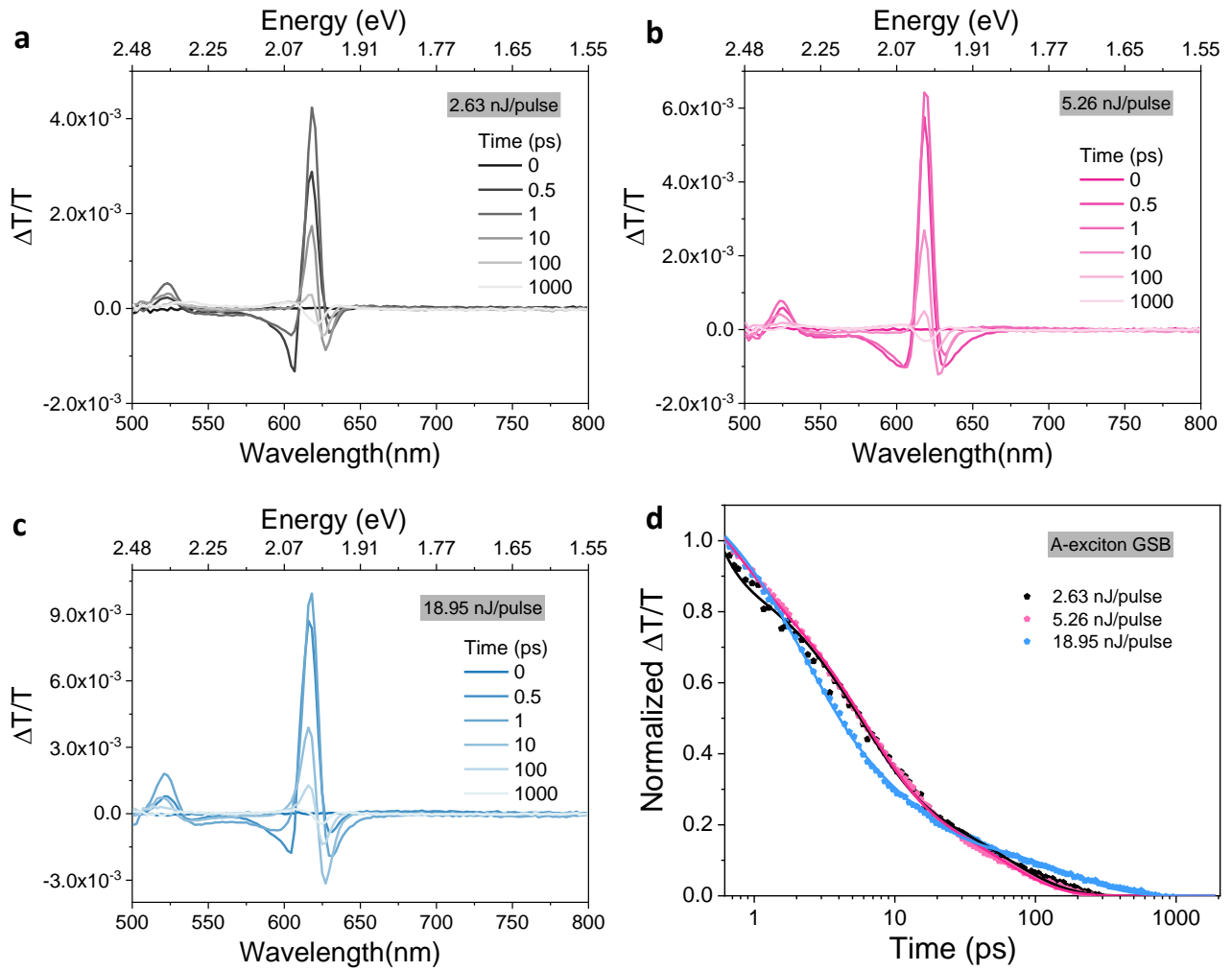


Figure S8. Fluence dependence of A-exciton resonance (excited at 610 nm) in pump-probe measurements. Pump-probe data of mechanically exfoliated pristine monolayer WS₂ sample with **a** 2.63 nJ/pulse, **b** 5.26 nJ/pulse, and **c** 18.95 nJ/pulse. **d** Normalized kinetics of A-exciton GSB of all samples.

Table S6. Fitting results for the rates at 610 nm excitation of mechanically exfoliated pristine WS₂ monolayer sample in pump-probe measurement.

Sample	A_1	τ_1 (ps)	A_2	τ_2 (ps)	A_3	τ_3 (ps)	$\langle \tau \rangle$ (ps)
2.63 nJ/pulse	2.68	0.18	0.67	5.5	0.29	62	6
5.62 nJ/pulse	0.44	0.47	0.68	5.7	0.29	55	14
18.95 nJ/pulse	0.68	1.93	0.37	10.0	0.18	167	29

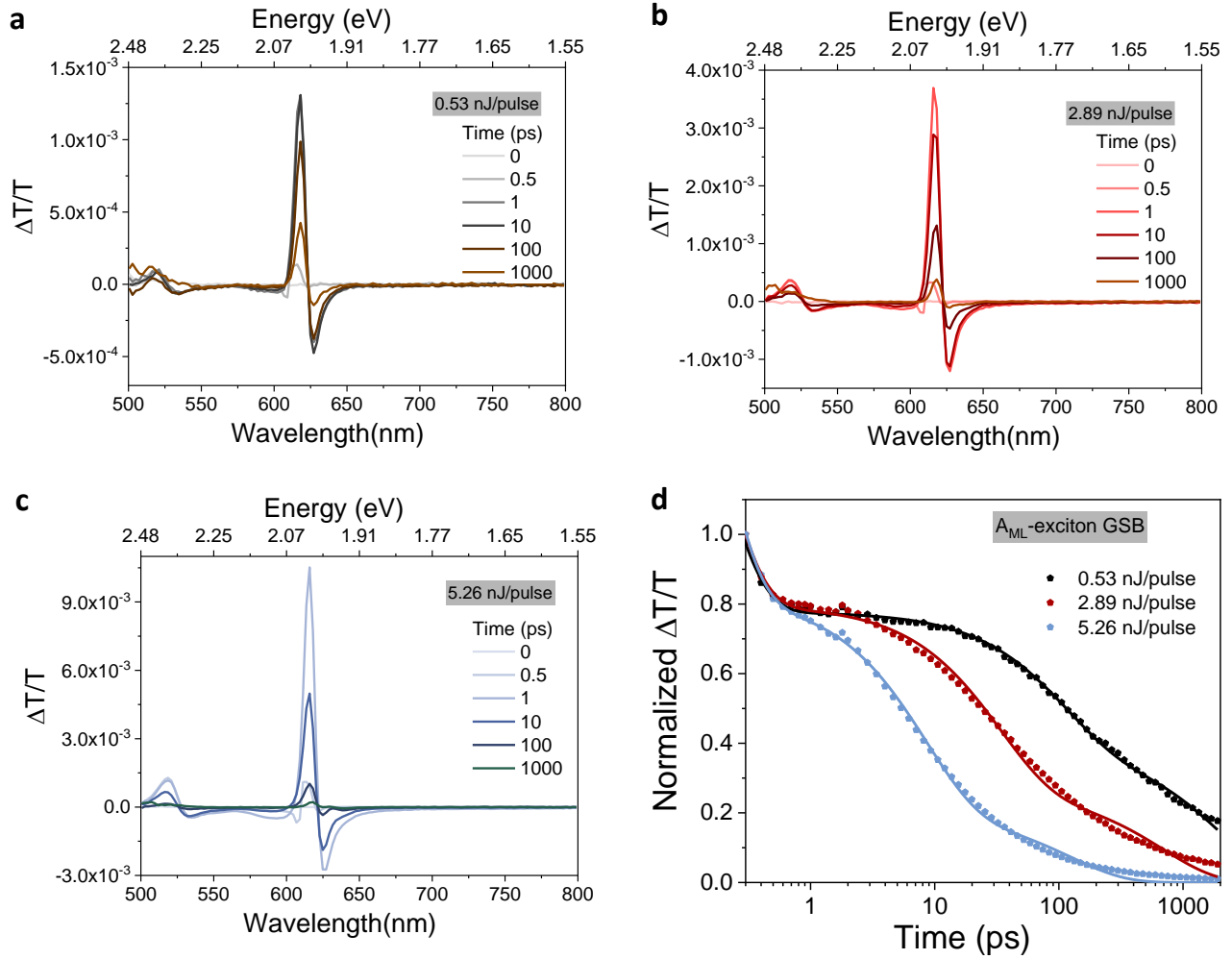


Figure S9. Fluence dependence of A-exciton resonance (excited at 610 nm) in mechanically exfoliated Li-TFSI treated monolayer WS₂ sample. Pump-probe data with **a** 0.53 nJ/pulse and **b** 2.83 nJ/pulse. **c** 5.26 nJ/pulse **d** Normalized kinetics taken at A_{ML}-exciton GSB of all samples.

Table S7. Fitting results for the rates at 610 nm excitation of mechanically exfoliated Li-TFSI treated WS₂ monolayer sample in pump-probe measurement.

Sample	A ₁	τ ₁ (ps)	A ₂	τ ₂ (ps)	A ₃	τ ₃ (ps)	$\langle\tau\rangle$ (ps)
0.53 nJ/pulse	1.77	0.14	0.39	108	0.39	2024	324
2.83 nJ/pulse	2.05	0.13	0.26	688	0.54	32.8	70
5.26 nJ/pulse	2.62	0.12	0.62	8	0.20	126	9

6. Reference

1. Tainter, G. D. *et al.* Long-Range Charge Extraction in Back-Contact Perovskite Architectures via Suppressed Recombination. *Joule* **3**, 1301–1313 (2019).
2. Allardice, J. R. *et al.* Engineering Molecular Ligand Shells on Quantum Dots for Quantitative Harvesting of Triplet Excitons Generated by Singlet Fission. *J. Am. Chem. Soc.* **141**, 12907–12915 (2019).
3. Backes, C. *et al.* Production of highly monolayer enriched dispersions of liquid-exfoliated nanosheets by liquid cascade centrifugation. *ACS Nano* **10**, 1589–1601 (2016).